Structure of the Stark recurrence spectrum

R. V. Jensen, H. Flores-Rueda,* J. D. Wright, M. L. Keeler,† and T. J. Morgan
Department of Physics, Wesleyan University, Middletown, Connecticut 06459
(Received 10 May 2000; published 16 October 2000)

The primary goal of research in ''quantum chaos'' is to explore the extent to which the methods and natural intuition of classical mechanics can be used to elucidate the complex and often surprising behavior of large quantum systems. Much recent work is based on the deep connections between classical periodic (or closed) orbits and the quantum spectrum revealed by semiclassical ''trace formulas.'' These ideas have important applications in the analysis of the ''recurrence spectrum'' of Rydberg atoms in strong static electric fields in which the measured peaks are associated with individual classical periodic orbits. Here we present detailed experimental measurements of the recurrence spectrum for $n=15$–25, singlet and triplet, $m=0$, 1, helium Rydberg atoms and we provide a purely quantum-mechanical explanation for the structure of the recurrence spectrum based on the regularities of the Stark photoabsorption spectrum. This analysis serves to demystify these (still complex) representations of the quantum spectrum; provides new insight into the functional differences between hydrogen and helium Rydberg atoms in strong fields; and reemphasizes the remarkable correpondence between the classical and quantum theory for these systems.

PACS number(s): 32.60.+i, 32.80.−t, 03.65.Sq

I. INTRODUCTION

An understanding of the correspondence between classical and quantum mechanics played a key role in the foundations of quantum theory and continues to be a subject of great interest today. It is particularly important for describing the physical behavior of systems that lie at the interface between the classical and quantum world, Rydberg atoms, large molecules, and mesoscopic electronic devices. At these new frontiers of scientific research the quantum theory can be very complicated and the corresponding classical theory is often chaotic. As a consequence, this resurgence of interest in semiclassical physics is often referred to as the study of ''quantum chaos.''

The primary goal of these (post-modern [1]) studies is to explore the extent to which the methods and natural intuition for classical mechanics can be used to elucidate the complex, and often surprising behavior of large quantum systems. Much recent theoretical work has built upon the deep connections between classical periodic or closed orbits and the quantum spectrum developed in the early 1970s by Gutzwiller [2] and by Berry and Tabor [3]. These mathematical methods have been developed into practical tools for detailed calculations of observable properties of physical systems (for direct comparison with experiment) by Delos [4,5], Heller [1,6], and others. In particular, the closed orbit theory for the calculation of the photo-absorption spectrum of complex, nonintegrable quantum systems, developed by Delos and his co-workers [4,5], has proven to be a valuable tool for interpreting the experimental measurements of the quantum spectra of Rydberg atoms in strong magnetic and electric fields in the laboratories of Welge [7,8], Kleppner [9,10], Hogervorst [11,12], and Morgan [13–15].

In these semiclassical ''trace formulas,'' the classical and quantum theories provide complementary descriptions of the complex physical systems—each quantum-mechanical energy level can be associated with a family of classical trajectories [2] and regularities in the complex quantum spectrum can often be associated with a single classical perodic or closed orbit [3]. Consequently, the classical mechanics may be used to provide extra insight into the properties of a quantum system with a complex spectrum, and conversely, the quantum theory (or experiment) may provide novel insight into the corresponding classical dynamics. This ''complementarity principle'' is the essential foundation for ''quantum chaos'' research at this interface between the classical and quantum worlds.

One important tool for studying this classical-quantum correspondence is the experimental measurement of the ''recurrence spectrum'' of a Rydberg atom in a strong static field. The usual Zeeman spectrum of a Rydberg atom in a strong magnetic field or the Stark spectrum of a nonhydrogenic atom in a strong static electric field is very complex with many avoided level crossings, resembling a bowl of spaghetti. However, if the spectrum is measured using ''scaled spectroscopy'' which constrains the level energies to scale with the applied field in such a way as to keep the classical Hamiltonian invariant, then regularities in the complex spectrum may emerge that can be associated with individual classical periodic orbits.

For example, in the recent experiments of Keeler and Morgan [13–15], the scaled energy spectrum, $\epsilon=|E|/\sqrt{F}=\text{const}$, was measured as a function of $w=1/F^{1/4}$ for helium Rydberg atoms excited to energies E (with respect to the zero field-ionization limit) in strong static electric fields F. These strange variables are dictated by the scaling properties of the classical Hamiltonian for the Rydberg electron moving in a Coulomb field with an applied static field. This scaled spectroscopy requires that the laser excitation energy be

*Permanent address: Instituto De Fisica, Universidad De Guanajuato, Mexico.
†Present address: Physics Department, University of Wisconsin, Madison, WI 53706.

shifted with the applied electric field to keep the scaled energy ϵ fixed.

When this still complicated, scaled photoabsorption spectrum is Fourier transformed with respect to w, we get a much simpler ''recurrence spectrum'' in which relatively few peaks appear. For $m=0$ hydrogen these lines in the recurrence spectrum are readily assigned to the scaled classical actions S, of individual classical orbits that start at the nucleus and return to the nucleus. In hydrogen these closed orbits are reflected by the Coulomb potential and retrace their paths completing a periodic orbit. The classical actions of these ''recurring'' orbits (and their integer multiples corresponding to the repetition of these orbits) define the ''recurrence spectrum'' that provides a complementary description to the usual energy spectrum.

While this program can be carried out numerically for hydrogen atoms, where there are no (nonrelativistic) avoided Stark levels, the experimentally measured recurrence spectrum for helium Rydberg atoms provides an interesting opportunity to study the effects of the broken Coulomb symmetry (due to the core electron) as well as the electron-spin interaction (due to Pauli exclusion) on the structure of the recurrence spectrum and the associated periodic orbits.

Figure 1 displays the calculated recurrence spectrum [15] for $m=0$ hydrogen and the measured recurrence spectrum [14,15] for the $m=0$ singlet and triplet states of helium Rydberg atoms with principle quantum numbers $n=15$–25. The strong static fields used in the calculations and experiments correspond to scaled energies ranging from $\epsilon=3.5$ to the classical ionization limit, $\epsilon=2$. Remarkably, all three recurrence spectra are very similar. All three exhibit a series of curved lines running from the top to the bottom of the graph that vary in intensity in distinct bands running from the lower left to the upper right. In Keeler and Morgan's previous work [13–15], the lines in the hydrogen recurrence spectrum have been assigned to individual classical closed orbits (and their repetitions) and the rise and fall of intensities have been roughly correlated with the bifurcation points of these orbits (where the periodic orbits change stability).

The strong similarity between the $m=0$ helium and hydrogen ''recurrence maps'' suggests that the origin of much of the structure in the helium recurrence maps is the same as in hydrogen. The most notable differences between hydrogen and helium is the appearance of a new band of enhanced intensity in the helium recurrence spectra that appears between the third and fourth diagonal band (read from left to right) of the hydrogen recurrence map and the comensurate reduction of the intensity of the third hydrogenic band.

These new peaks in the recurrence spectra have been previously identified with the emergence of core-scattered classical orbits that lead to contributions from combinations of the hydrogenic ''uphill'' and ''downhill'' periodic orbits in the static electric field [10]. Unfortunately, the extension of the closed orbit theory to helium atoms is complicated by the fact that there are typically several combination orbits that may contribute semiclassically to the additional helium line intensities and to the depletion of the hydrogenic line intensities [14,15].

The calculated hydrogen recurrence spectra and measured

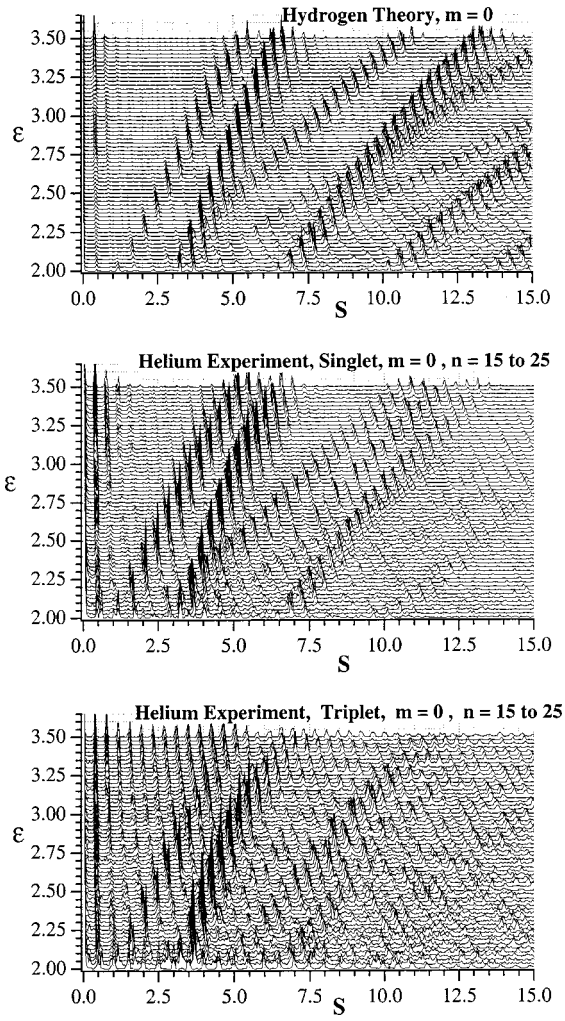

FIG. 1. Comparison of the $m=0$ Stark recurrence maps for hydrogen and helium Rydberg atoms in strong static electric fields with scaled energies ϵ, between 3.5 and 2.0 and scaled actions, S, up to 15. These recurrence maps are determined by the Fourier transforms of (a) the calculated hydrogen photoabsorption spectrum for $n=15$–20, (b) the measured photoabsorption for the singlet helium states with $n=15$–25, and (c) the measured photoabsorption for the helium triplet states with $n=15$–25.

helium (singlet and triplet) spectra [13] for $m=1$ Rydberg atoms shown in Fig. 2 provide even greater challenges to this semiclassical interpretation of the quantum spectra. The overall appearance of the $m=1$ recurrence maps in Fig. 2 is much simpler than the $m=0$ maps shown in Fig. 1 with fewer bands of enhanced intensity. However, these bands can no longer be directly associated with bifurcations of closed orbits since there are no real closed orbits that start from the nucleus and return because of the angular momentum barrier at the nucleus. Again the hydrogen and helium recurrence maps are very similar. The primary differences between hydrogen and helium are the regular modulations of the second and third bands of the helium recurrence maps that are most prominent in the triplet case, Fig. 2(c) [13].

One of the primary goals of this paper will be a return to the guiding ''complementarity principle'' for this research to search for the quantum mechanisms that explain the similar-

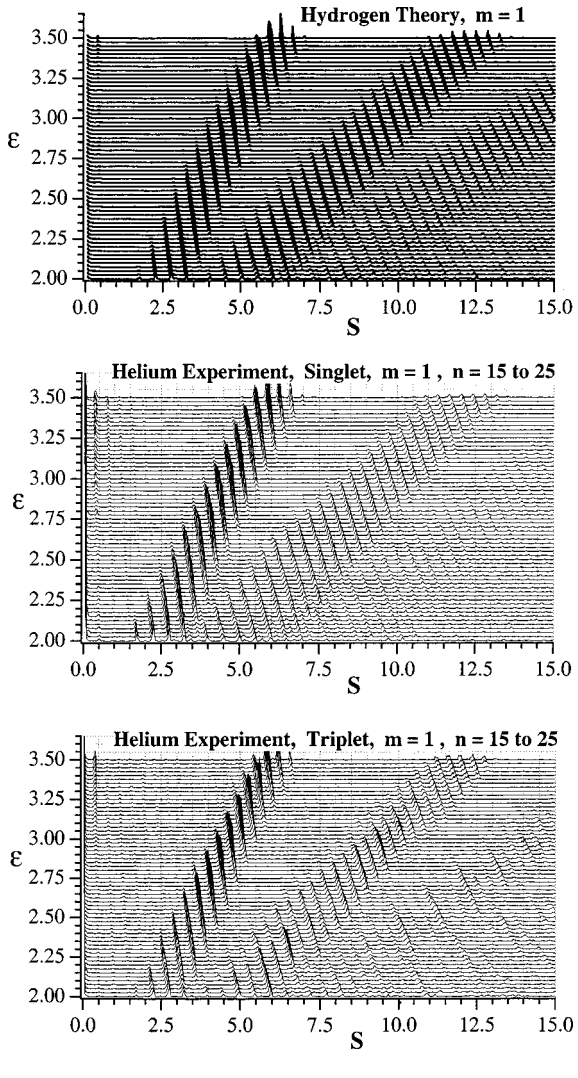

FIG. 2. Comparison of the $m=1$ Stark recurrence maps for hydrogen and helium Rydberg atoms in strong static electric fields with scaled energies ϵ, between 3.5 and 2.0 and scaled actions, S, up to 15. These recurrence maps are determined by the Fourier transforms of (a) the calculated hydrogen photoabsorption spectrum for $n=15$–20, (b) the measured photoabsorption for the singlet helium states with $n=15$–25, and (c) the measured photoabsorption for the helium triplet states with $n=15$–25.

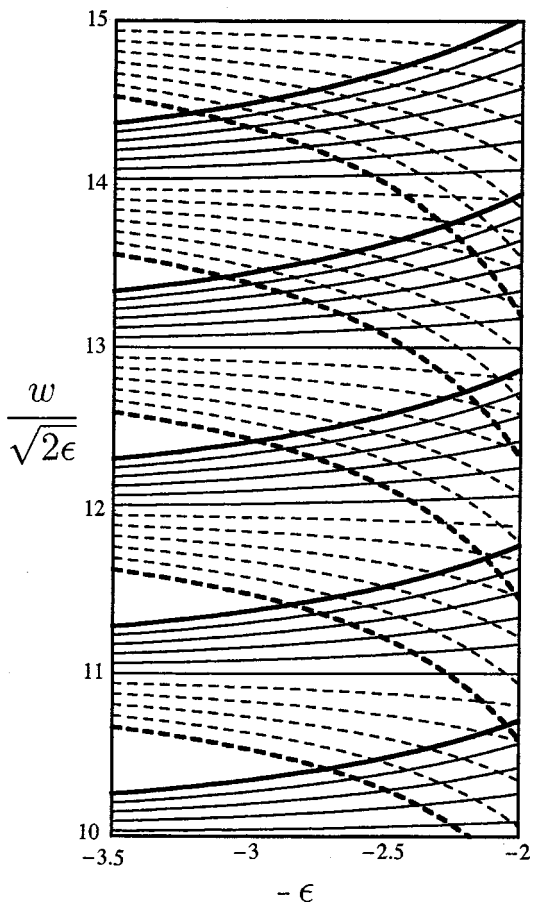

FIG. 3. The scaled Stark eigenvalues w, for the hydrogen, $m=0$, $n=10$–15 states are plotted as a function of the scaled-energy parameter $-\epsilon$, ranging from -3.5 to -2.0. The solid curves correspond to ''blue''shifted levels and the dashed curves to the ''red'' shifted levels. The extremal states for each n are highlighted to emphasize the periodic spacing.

ites and differences between the hydrogen and helium recurrence spectra. This analysis leads to simple quantum as well as classical descriptions of the intricate structure of the recurrence maps displayed in Figs. 1 and 2. This complementary approach serves to demystify these (still complex) representations of the quantum spectrum. It provides new insight into the functional differences between hydrogen and helium Rydberg atoms in strong fields and reemphasizes the remarkable correspondence between the classical and quantum theory for these systems. Finally, this work paves the way for the analysis of more ambitious experimental studies of more complex atomic and molecular Rydberg states in strong fields.

In Sec. II, we calculate the scaled Stark spectrum for the $m=0$ states of hydrogen and show that careful analysis of the periodicities in the scaled photoabsorption spectrum accounts for both the fine-scale and large-scale structure of the $m=0$ hydrogen recurrence map shown in Fig. 1(a). A comparison with the predictions of the semiclassical closed orbit theory illustrates the virtues and limitations of these complementary approaches. Then our analysis is extended to the $m=1$ case in Sec. III, where the semiclassical closed orbit theory breaks down. Again our analytical results agree well with the calculated hydrogen $m=1$ recurrence map as well as our experimently measured helium singlet and triplet $m=1$ recurrence maps. In Sec. IV, the effects of avoided level crossings in the helium Stark spectrum are introduced into our analysis of the level periodicities to offer a simple explanation for the key differences between the hydrogen and helium $m=0$ recurrence maps in terms of the avoided crossings between the helium Stark levels. These differences have been previously described in the semiclassical closed orbit theory by invoking the contributions of ''core scattered'' classical orbits [14]. Finally, Sec. V provides a summary of our results and discusses remaining puzzles relating to subtle differences in the hydrogen and helium $m=1$ recurrence maps.

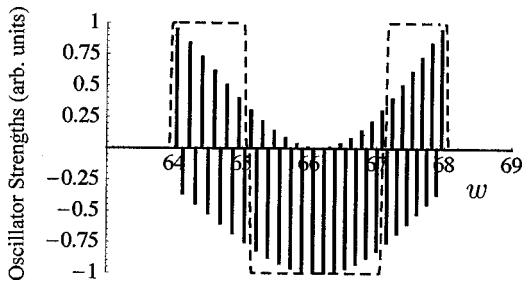

FIG. 4. The theoretical photoabsorption oscillator strengths for the hydrogen $n=25$ Stark manifold at $\epsilon=3.5$ are plotted as a function of w for the $m=0$ (top) and $m=1$ (bottom) states. For $m=0$, the oscillator strengths are peaked near the extremal red and blue substates and for $m=1$ the oscillator strengths are peaked near the center of the manifold [16,17]. The dotted step functions show the approximate oscillator strengths used in our analytical calculations of the scaled hydrogen, $m=0$ and 1 recurrence spectra.

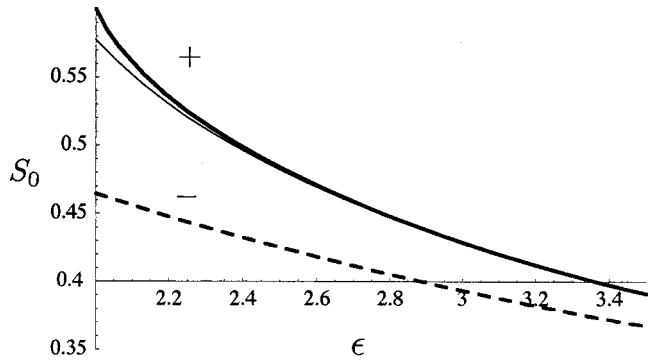

FIG. 5. The actions of the 1D classical uphill (+) and downhill (−) actions, Eq. (4), are plotted as functions of ϵ by the heavy solid and dashed lines, respectively. The thin solid curve shows the simple analytical approximation to the uphill action integal provided by quantum mechanics, Eq. (8). The analytical approximation for the downhill action is indistinguishable from the exact classical action in this figure.

II. HYDROGEN RYDBERG ATOMS, $m=0$

In atomic units the first-order Stark energy levels in hydrogen are

$$-E=-\frac{1}{2n^2}+\frac{3}{2}n\kappa F, \tag{1}$$

where $\kappa\equiv(n_1-n_2)$ is the electric quantum number expressed in terms of the parabolic quantum numbers n_1 and n_2 defined by $n=n_1+n_2+|m|+1$. The scaled Stark energies $\epsilon\equiv|E|/\sqrt{F}$, are then determined by

$$-\epsilon=-\frac{w^2}{2n^2}+\frac{3}{2}\frac{n\kappa}{w^2}, \tag{2}$$

where $w\equiv F^{-1/4}$. For a fixed scaled energy ϵ, the Stark spectral lines correspond to discrete values of w that are solutions to Eq. (2) for different principal quantum numbers, n, and electric quantum numbers κ. [In fact, Eq. (2) has four roots, so we must choose the real, positive roots, w, that are closest to the field-free value, $n\sqrt{2\epsilon}$.] Figure 3 displays the ''blue'' and ''red'' w levels as a function of $-\epsilon$ for $n=10$–15. (Note that for weak fields corresponding to large values of ϵ, $w/\sqrt{2\epsilon}$ converges to the principal quantum numbers $n=10$–15.)

The usual procedure for generating a theoretical recurrence spectrum is to associate an amplitude with each energy level that is proportional to the oscillator strengths for the photoexcitation of these excited states from the initial state. For $m=0$, these oscillator strengths are peaked near the extremal levels with an expected distribution of the form $\sin^2(\kappa/n)$ [16,17] shown in Fig. 4 (top). Then the recurrence spectrum is generated by numerically performing a Fourier transform of these sequences of lines as a function of w for each ϵ. Figure 1(a) displays this weighted Fourier transform of the hydrogenic energy levels from $n=15$–25 for values of ϵ from 3.5 to 2. This is the so-called Stark recurrence map.

The semiclassical ''closed orbit'' theory [4,10] predicts that each of the peaks in the Stark recurrence map corresponds to the scaled actions S of closed orbits in the classical theory. According to the closed orbit theory, when a photon is absorbed by the atom in an electric field forming a Rydberg state, the electron initially becomes a near zero-energy outgoing Coulomb wave. Beyond a sufficient distance from the nucleus, this wave propagates semi-classically along classical trajectories in the combined Coulomb and static field. The classical trajectories that return to the nucleus provide opportunities for the electron wave function to interfere with the outgoing wave forming an ''atomic interferometer'' that is responsible for the structure in the photoabsorption spectrum. Each closed orbit and its repetitions contribute an oscillatory term to the photoabsorption spectrum. When the spectrum is recorded at constant scaled energy, the periodicities in w and the associated peaks in the Fourier transform (recurrence spectrum) correspond to the classical actions of these closed orbits.

Because the oscillator strengths for the photoexcitation of the $m=0$ states are peaked near the extremal states, the classical scaled actions associated with the periodicities in the photoabsorption spectrum are well approximated by the scaled actions of the up- and down- hill orbits parallel to the z axis determined by the scaled, one-dimensional Hamiltonian

$$-\epsilon=\frac{p^2}{2}-\frac{1}{z}\pm z, \tag{3}$$

where $z\geqslant 0$ and p are scaled position and momentum variables and the $\pm$ correspond to the up- and down-hill motion, respectively. Then, evaluating the the classical scaled actions $S\equiv(1/2\pi)\int p\,dz$, we get

$$S^{\pm}=\frac{1}{\pi}\int_0^{z^{\pm}}\sqrt{2\left(\frac{1}{z}\mp z-\epsilon\right)}\,dz, \tag{4}$$

where the one-dimensional classical orbits are reflected at the origin and reach a maximum excursion $z^{\pm}=(\mp\epsilon\pm\sqrt{\epsilon^2\pm 4})/2$. Although these action integrals can be formally evaluated in terms of elliptic integrals [17], it is more

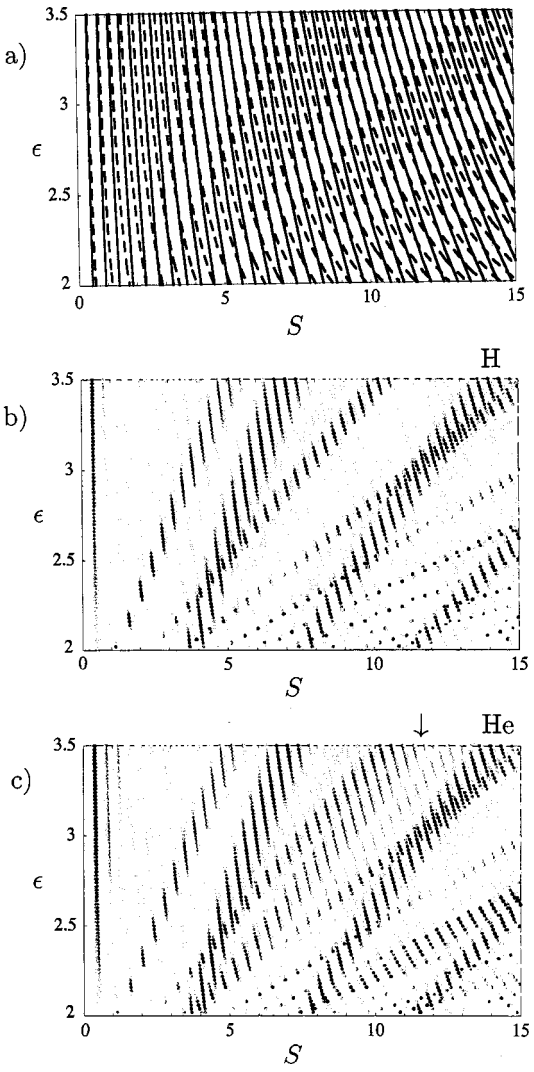

FIG. 6. (a) The bare $m=0$ recurrence spectrum generated by periodicities of the extremal red and blue states alone is plotted in the S-ϵ plane. The solid curves show the fundamental frequency S_0^+ for the blue extremal states and its harmonics, and the dashed curves show the fundamental frequency S_0^- for the red extremal states and its harmonics. (b) The modulated bands in the full recurrence spectrum arise from additional intereference of the red and blue Stark substates. This figure shows the analytical estimates for the locations of the substate interference bands using a step-function oscillator strengths as shown in Fig. 4. This theoretically derived recurrence map successfully describes most of the small and large-scale structure of the hydrogen and helium recurrence maps shown in Fig. 1(c). When avoided crossings are included in the analytical estimates for the extremal Stark level substate spacings, a new interference band (indicated by the arrow) arises from the ''purple'' substates that agrees well with the novel band in the measured helium, $m=0$, recurrence spectrum shown in Fig. 1.

convenient (and sometimes more accurate) to simply evaluate the integrals numerically for each value of ϵ as shown in Fig. 5. The individual peaks for constant ϵ in the hydrogen recurrence spectra displayed in Fig. 1(a) correspond very closely to integer multiples of these classical scaled actions shown in Fig. 5.

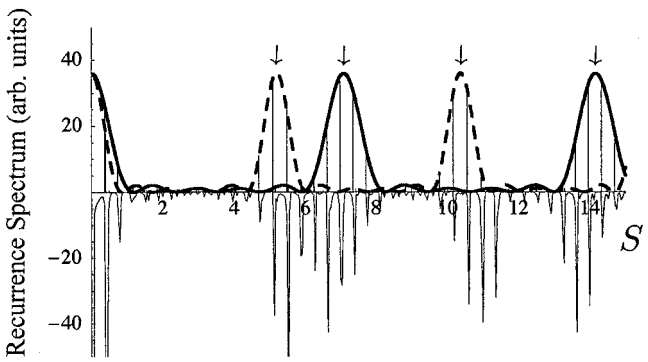

FIG. 7. Comparison of the modulated fundamental peaks from the present analysis (top) with the calculated hydrogen recurrence spectrum (bottom) for $\epsilon=3.5$. The dashed top curve shows the predicted envelope for the downhill red states and the solid top curve shows the envelope for the uphill blue states. Our approximate analytical results, using the simplified step-function oscillator strengths shown in Fig. 4, accurately defines the outer edge of the prominent bands in the recurrence spectrum. A more accurate description requires the numerical Fourier transform of the photoabsorption spectrum described in the Appendix.

The closed orbit theory predicts further that the amplitudes of these peaks are greatly enhanced near ''bifurcation'' points where new closed orbits are created from the bifurcations of the parallel up- and down-hill orbits as the scaled energy is varied. For $m=0$ hydrogen Rydberg atoms in a static electric field, Courtney *et al.* [10] have carefully calculated the classical actions and bifurcation points for closed electron orbits that start at the nucleus and return. In fact, the (ϵ,S) loci for these bifurcations provide a good description of the outer boundaries of the first two enhanced bands of recurrence peaks and the outer boundaries of the subsequent bands can also be explained in terms of the harmonics of these bifurcations.

Much analytical and numerical work has been devoted to understanding the details of this correspondence; however, mathematically speaking, the peaks in the Fourier transform simply correspond to the frequencies associated with the periodicities in the scaled Stark spectrum like those highlighted in Fig. 3. In this paper, we will attempt to identify the origins of periodicities in the scaled Stark spectrum in order to analytically perform these Fourier transforms. Our Fourier analysis of the scaled Stark line spectrum for each value of ϵ resembles the description of a diffraction grating with periodically spaced slits. This approach provides an alternative, quantum-mechanical explanation for the locations and amplitudes of the peaks in the recurrence maps that complements the closed orbit theory and provides additional insight into the intricate structure of the quantum energy levels and their relationship to the classical dynamics.

The analysis of the periodicities in the Stark spectrum can be simplified by considering the limit of large n. Then, for $m=0$ the extremal ''blue'' state corresponds to $\kappa=n-1\approx+n$ and the extremal ''red'' state, to $\kappa=-n+1\approx-n$. In these limiting cases, the solutions of Eq. (2) are

$$w^+ = n\left(\epsilon + \sqrt{\epsilon^2+3}\,\right)^{1/2} \equiv n\Delta_0^+, \tag{5}$$

$$w^- = n\left(\epsilon + \sqrt{\epsilon^2-3}\,\right)^{1/2} \equiv n\Delta_0^-. \tag{6}$$

The extremal levels define the periodic framework for the Stark level structure shown in Fig. 3. For fixed values of the scaled energy ϵ, the periodicity of the extremal states (highlighted in Fig. 3) and of the adjacent substates should be readily apparent.

From Eqs. (5) and (6) the periods of the ''blue'' (+) levels and ''red'' (−) levels in w are approximately $\Delta^+ = \left(\epsilon + \sqrt{\epsilon^2+3}\,\right)^{1/2}$ and $\Delta^- = \left(\epsilon + \sqrt{\epsilon^2-3}\,\right)^{1/2}$, respectively. These well-defined periodic structures determine much of the fine structure of the Stark recurrence map. Approximating these sequences of lines as periodic δ functions, we can use the Poisson identity

$$\sum_{n=-\infty}^{\infty} \delta(w - n\Delta_0^{\pm}) = \sum_{k=-\infty}^{\infty} e^{i2\pi w k/\Delta_0^{\pm}} \tag{7}$$

to instantly perform the Fourier transform to determine the fundamental ''frequencies'' arising from these contributions to the scaled Stark spectrum. Motivated by the semiclassical closed orbit analysis, we call these frequencies the ''scaled actions'' S and we see from Eq. (7) that the Fourier transform of the extremal Stark lines with respect to w will contribute peaks in the recurrence spectrum at integer multiples of the scaled actions $1/\Delta_0^+$ and $1/\Delta_0^-$ shown in Fig. 6(a). A comparison of Fig. 1 and Fig. 6(a) shows that the fine structure of the peak locations in the calculated and measured recurrence maps are well-described by this simple analysis.

In a remarkable demonstration of the utility of the application of the ''reverse'' correspondence principle we find that this simple quantum-mechanical result for the inverse level spacings, Eqs. (5) and (6) provide excellent analytical approximations for the difficult classical action integrals, Eq. (4). In Fig. 5, the analytical expressions for the fundamental quantum frequencies

$$S_0^{\pm} = 1/\Delta_0^{\pm} = 1/\left(\epsilon + \sqrt{\epsilon^2 \pm 3}\,\right)^{1/2} \tag{8}$$

converge rapidly to the results for the classical action integrals, Eq. (4) with increasing ϵ.

Next we show that the large-scale banded structure in the Stark recurrence map in Fig. 1(a) can be simply described by the periodicities of the scaled Stark substates. The exterior framework provided by the extremal states is filled in with a lattice of substates corresponding to the intermediate values of the electric quantum number $\kappa = n-1, n-3, \ldots, -n+3, -n+1$ for $m=0$. The locations of these substates are determined by solving

$$-\epsilon = -\frac{w^2}{2n^2} + \frac{3}{2}\frac{n^2(1-x/n)}{w^2}, \tag{9}$$

for

$$w(n,x) = n\left[\epsilon + \sqrt{\epsilon^2 + 3 - 3\,(x/n)}\,\right]^{1/2}, \tag{10}$$

where $x \equiv n - \kappa = 1,3,5,\ldots,2n-1$.

First note that the substates near the edge of the Stark manifold have approximately the same periodicities as the corresponding extremal states. Consider first the blue-shifted states defined by Eq. (10) with $x = 1,3,5,$ to $n-1$ (if n is even) or n (if n is odd). If we fix x and differentiate Eq. (10) with respect to n, then

$$\begin{aligned}\Delta(n,x) &= dw(n,x)/dn = d[nw(1,x/n)]/dn \\ &= w(1,x/n) - w'(1,x/n)(x/n)\end{aligned} \tag{11}$$

since $\Delta n = 1$. Expanding Eq. (11) for small (x/n) gives

$$\begin{aligned}\Delta(n,x) &= w(1,0) + w'(1,0)(x/n) - w'(1,0)(x/n) \\ &\quad + O((x/n)^2) \\ &= w(1,0) + O((x/n)^2) \\ &\approx \left(\epsilon + \sqrt{\epsilon^2+3}\,\right)^{1/2},\end{aligned} \tag{12}$$

which is the blue extremal-state spacing, Δ_0^+, defined by Eq. (5).

Consequently, the Fourier transforms of these periodic ladders of adjacent blue and red substates will add coherently to the contributions from the extremal states alone. However, these substate ladders are displaced in w from the extremal states, which introduces a phase shift in the Fourier components associated with each family of substates.

To calculate the coherent contributions of the blue substates we can estimate the near extremal-substate spacings by evaluating the derivative of $w(n,x)$ with respect to x in the limit $(x/n) \to 0$,

$$\delta_0^+ = \left.\frac{dw(n,x)}{dx}\right|_{x=0} = \frac{-3}{4\sqrt{\epsilon^2+3}\left(\epsilon + \sqrt{\epsilon^2+3}\,\right)^{1/2}}. \tag{13}$$

Then the spacing between adjacent extremal substates ($x = 1,3,5,\ldots$) is approximately $2\delta_0^+$, since $\Delta x = 2$, independent of both n and x. These approximately uniform ''phase'' differences in the coherent sums of the Fourier components result in important destructive and constructive interferences, that depress the strength of some lines in the bare extremal recurrence spectrum in Fig. 6(a) and enhance others leading to the large-scale banded structure in Fig. 1(a).

Using the Poisson sum formula, Eq. (7), for each ladder of blue-shifted substates,

$$\sum_n \delta(w-nw(1,1/n))+\sum_n \delta(w-nw(1,3/n))+\sum_n \delta(w-nw(1,5/n))+\cdots$$

$$\approx\sum_n \delta(w-n\Delta_0^+-\delta_0^+)+\sum_n \delta(w-n\Delta_0^+-3\delta_0^+)+\sum_n \delta(w-n\Delta_0^+-5\delta_0^+)+\cdots$$

$$=\sum_k e^{i2\pi k(w-\delta_0^+)/\Delta_0^+}+\sum_k e^{i2\pi k(w-3\delta_0^+)/\Delta_0^+}+\sum_k e^{i2\pi k(w-5\delta_0^+)/\Delta_0^+}+\cdots$$

$$=\sum_k e^{i2\pi k(w-\delta_0^+)/\Delta_0^+}(1+e^{-i2\pi k2\delta_0^+/\Delta_0^+}+e^{-i2\pi k4\delta_0^+/\Delta_0^+}+\cdots), \tag{14}$$

the strength of each of the recurrence spectrum lines at scaled actions k/Δ_0^+ can be estimated by the square modulus of the geometric series

$$A^+(k,\epsilon)=|(1+e^{-i2\pi k2\delta_0^+/\Delta_0^+}+e^{-i2\pi k4\delta_0^+/\Delta_0^+}+\cdots)|^2$$
$$=\sin^2(2\pi Nk\delta_0^+/\Delta_0^+)/\sin^2(2\pi k\delta_0^+/\Delta_0^+), \tag{15}$$

where N is the number of substates contributing to the coherent sum. $A_+(k,\epsilon)$ is the familiar diffraction grating function that exhibits strong constructive interference peaks corresponding to integer values of $k2\delta_0^+/\Delta_0^+$ with a height N^2 and with a width proportional to $1/N^2$.

Similar results are obtained from the periodicity of the substates near the extremal ''red'' state $\kappa=-n+1$, which have an approximately constant periodicity in w of Δ_0^-. In this case the locations of the red substates can be computed using Eq. (10) with $x=-1,-3,-5,\ldots$. Then taking the derivative of Eq. (10) with respect to $-x$ we get an estimate for the displacements of the extremal red states $2\delta_0^-$, where

$$\delta_0^-=\frac{3}{4\sqrt{\epsilon^2-3}\left(\epsilon+\sqrt{\epsilon^2-3}\right)^{1/2}}. \tag{16}$$

These redshifted substates lead to constructive intereference in the recurrence spectrum for scaled actions corresponding to integer values of $k2\delta_0^-/\Delta_0^-$ described by the diffraction grating function

$$A^-(k,\epsilon)=\sin^2(2\pi Nk\delta_0^-/\Delta_0^-)/\sin^2(2\pi k\delta_0^-/\Delta_0^-), \tag{17}$$

where N is the number of substates contributing to the coherent sum.

Expressed in terms of the scaled actions, these resonant conditions for constructive interference predict that the bare recurrence peaks at integer multiples of $S_0^\pm=1/\Delta_0^\pm$ will be enhanced near integer multiples of

$$s_0^\pm=1/2|\delta_0^\pm|=\frac{2}{3}\sqrt{\epsilon^2\pm3}\left(\epsilon+\sqrt{\epsilon^2\pm3}\right)^{1/2}, \tag{18}$$

and suppressed in between. In general, the precise shape of the envelope function that describes the modulation of the heights of the bare recurrence spectrum depends on both the distribution of oscillator strengths as a function of the electric quantum number κ, [$\sin^2(\kappa/n)$ for $m=0$] shown in Fig. 4, as well as the slow variation of $\delta_0^\pm$ with increasing κ. (See the appendix.) However, for a rough comparison with the numerically calculated recurrence spectrum from the Fourier transform of the scaled-energy Stark spectrum, we have kept only the extremal $N=6$ ''blue'' and ''red'' substates in each Stark manifold, assigned them a constant oscillator strength, and neglected any gradual change in the substate spacings. These assumptions correspond to the approximate, step-shaped, oscillator strength distribution shown in Fig. 4 (top).

For example, a comparison in Fig. 7 of this analytical estimate of the recurrence spectrum band structure (top) with the calculated hydrogen recurrence spectrum (bottom) for $\epsilon=3.5$ shows that this approximate model provides a good description of the large-scale modulations of the data. The top graph in Fig. 7 shows the envelope functions for the red and blue substate interferences (dashed and solid curves, respectively) that modulate the bare recurrence spectrum (stick spectrum) defined by the extremal states alone. Since $s_0^-=1/2|\delta_0^-(3.5)|\simeq5$ and $s_0^+=1/2|\delta_0^+(3.5)|\simeq7$, the first two bands of enhanced recurrence line strength arise from the diffraction grating functions for the red and blue substates, respectively. Subsequent peaks in the diffraction functions arise from higher harmonics of these substate frequencies. (As long as the locations of the constructive interference of the red and blue states are disjoint we need not be concerned about the additional constructive and destructive interference between the red and blue contributions.)

In contrast, the classical closed-orbit theory predicts that the recurrence spectrum is enhanced near the scaled actions where the classical up- and down-hill orbits undergo bifurcations that must be determined from a numerical analysis of this classical nonlinear dynamical system [18]. For $\epsilon=3.5$, the actions of the classical orbits that are closest to bifurcation points are indicated by the arrows in Fig. 7. Moreover, to account for detailed modulations of the recurrence spectrum shown in Fig. 7, the closed-orbit theory must be further augmented by a uniform approximation for the semiclassical wave function in the vicinity of the singularity due to the classical bifurcation [19]. Finally, we note that closed-orbit theory offers no simple explanation for the enhanced recurrence peaks near scaled action of zero where there are no

classical bifurcations. However, this enhanced recurrence strength at small actions is well-described by the diffraction grating functions from our analytical treatment of the Stark substate periodicities (as shown in Fig. 7).

These estimates for the diffraction grating functions generated by the substate periodicities were used in Fig. 6(b) to model the modulation of the bare recurrence spectrum in Fig. 6(a). A comparison of the exact recurrence map for $m=0$ hydrogen in Fig. 1(a) with Fig. 6 shows that this simple analysis of the quantum periodicities provides an excellent description of both the fine-scale and large-scale structure of the full recurrence map.

III. HYDROGEN RYDBERG ATOMS, $m=1$

Our approach to analyzing the Stark recurrence spectrum is easily extended to the description of the $m=1$ hydrogen spectrum even though there are no closed orbits that start and end at the nucleus because of the $m=1$ angular momentum barrier. Because our measured helium recurrence maps, Figs. 2(b) and 2(c), are remarkably similar to hydrogen, we will focus again on the description of the fine-scale and large-scale structure of the Stark recurrence map in terms of periodicities in the hydrogen photoabsorption spectrum. For $m=1$ hydrogen the first-order scaled Stark levels are still determined by Eq. (10) but now $x \equiv n-\kappa = 2,4,6,\ldots,2n-2$. In addition, the oscillator strengths for photo-absorption are peaked near the center of the Stark manifold with a distribution proportional to $\cos^2(\kappa/n)$ [16,17] as shown in Fig. 4 (bottom). So we must analyze the periodicities of the scaled Stark levels near the center of the manifold to determine the structure of the Stark recurrence spectrum.

For even n there is one scaled-energy level, $w(n,n) = n\sqrt{2\epsilon}$, with $x=n$ that lies at the center of the Stark manifolds and is unperturbed by the applied field as shown in Fig. 8. For odd n this center level is missing. Therefore, this central level will contribute to the amplitude of the $1/\sqrt{8\epsilon}$ frequency (and its harmonics) in the Fourier transform of the scaled Stark spectrum. However, since only a single level contributes from each even n manifold, this contribution to the recurrence spectrum will be weak.

In contrast, many levels near the center of each manifold will contribute to the fundamental Fourier components. For each x the spacing from one n manifold to the next is approximately constant. For the ''blue'' states this constant spacing can be determined by differentiating Eq. (10) with respect to n for fixed x and then taking the limit as $x \to n$. This gives a fundamental $m=1$, ''blue'' level spacing of

$$\Delta_1^+ = \frac{8\epsilon^2+3}{4\sqrt{2}\epsilon^{3/2}}. \tag{19}$$

A similar analysis of the red states for $m=1$ gives

$$\Delta_1^- = \frac{8\epsilon^2-3}{4\sqrt{2}\epsilon^{3/2}}. \tag{20}$$

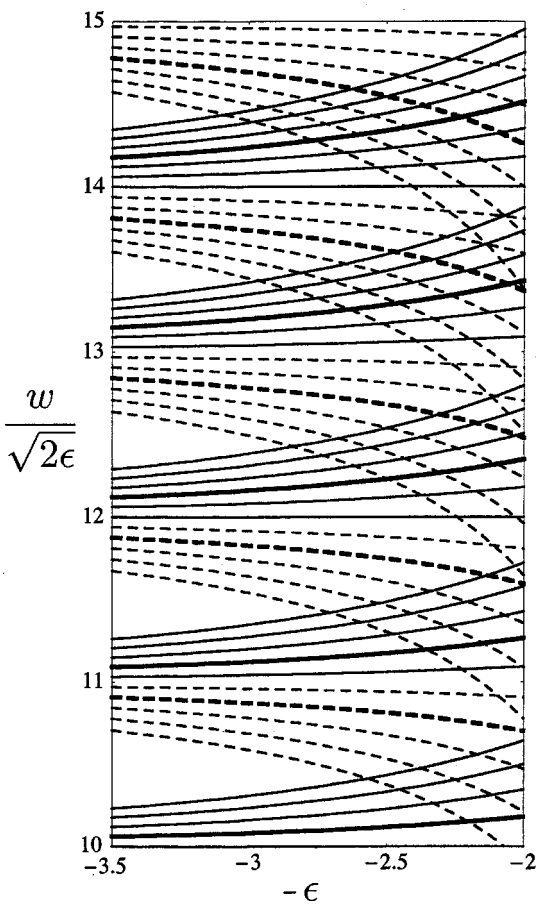

FIG. 8. The scaled Stark eigenvalues w for the hydrogen, $m=1$, $n=10$–15 states are plotted as a function of the scaled energy parameter, $-\epsilon$, ranging from -3.5 to -2.0. The solid curves correspond to ''blue''shifted levels and the dashed curves, to ''red'' shifted levels. The central blue and red states with fixed $x=\pm 8$ are highlighted for each n to emphasize the periodic spacing.

Then the Fourier transforms of these periodic ladders of adjacent blue and red substates will add coherently to generate the bare recurrence spectrum displayed in Fig. 9(a) with peaks at integer multiples of

$$S_1^{\pm} = 1/\Delta_1^{\pm}. \tag{21}$$

However, these substate ladders near the center of the manifold are displaced in w from the extremal states by $x\delta^+$, where δ^+ is estimated by differentiating Eq. (10) with respect to x for fixed n and taking the limit $x \to n$,

$$\delta_1^+ = \frac{-3}{4\sqrt{2}\epsilon^{3/2}}. \tag{22}$$

Similarly, the red substate spacing for $m=1$ is

$$\delta_1^- = \frac{3}{4\sqrt{2}\epsilon^{3/2}}. \tag{23}$$

These approximately uniform ''phase'' differences in the coherent sums of Fourier components result in important de-

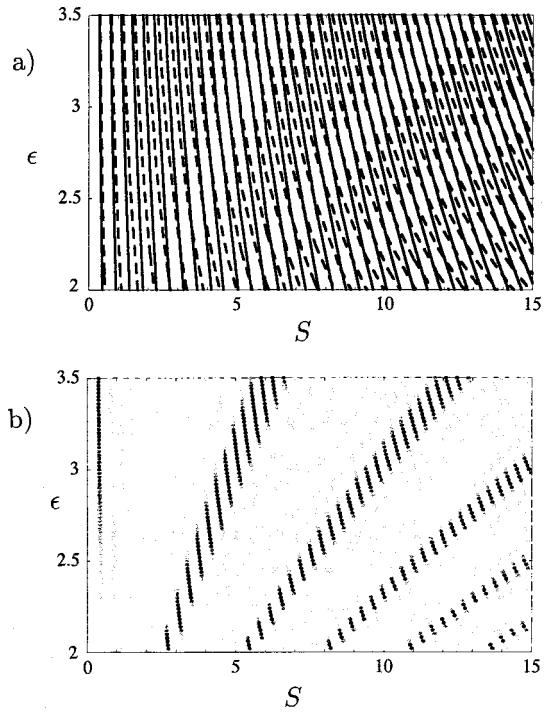

FIG. 9. (a) The bare $m=1$ recurrence spectrum generated by periodicities of the central red and blue states alone. The solid curves correspond to the fundamental frequency S_1^+ for the blue central states and its harmonics. The dashed curves to the fundamental frequency S_1^- for the red central states and its harmonics. (b) The modulated bands in the full recurrence spectrum arise from additional interferences of the red and blue Stark substates, respectively. This figure shows the analytical estimates for the locations of the substate interference bands using the step-function oscillator strengths shown in Fig. 4. This theoretically derived recurrence map successfully describes most of the the small and large scale structure of the hydrogen and helium recurrence maps shown in Fig. 2.

structive and constructive interferences that depress the strength of some lines in the bare recurrence spectrum for $m=1$ and enhance others.

As in the $m=0$ case, the destructive and constructive interference that arises from these substates can be characterized by simple diffraction grating funcions. When these modulations of the bare recurrence specturm for both the red and the blue states are taken into account, we arrive at the recurrence map shown in Fig. 9(b). The corresponding fundamental frequencies $1/\Delta_1^{\pm}$ and their harmonics account for the fine structure in the calculated recurrence spectrum and the substate frequencies

$$s_1^{\pm}=1/2|\delta_1^{\pm}|, \tag{24}$$

and their harmonics describe the bands of enhanced Fourier amplitude shown in Fig. 9(b). Since the red and the blue substate frequencies are the same in the $m=1$ case, the bands of constructive interference for the red and blue states coalesce, which accounts for the relative simplicity in appearance of the $m=1$ hydrogen Stark recurrence maps in Figs. 2(a).

A comparison of Figs. 2(a) and 9(b) shows that this simple analysis of the quantum periodicities provides an excellent description of the $m=1$ Stark recurrence spectra. In contrast, there is no semiclassical closed orbit theory for the $m=1$ case [20]. The locations of the peaks in the hydrogen Stark recurrence spectrum do not corespond to the actions of any real closed orbits and the bands of constructive interference are not delimited by the bifurcations of any real classical trajectories. However, in another remarkable application of the correspondence principle Main [21] has recently shown that the low action peaks in the $m=1$ Stark recurrence spectrum do correspond to the actions of imaginary classical orbits propagated with complex momenta [22]. This analytic continuation of semiclassical mechanics to complex trajectories is worthy of much further study.

IV. HELIUM RYDBERG ATOMS, $m=0$

Finally, the strong similarity of the recurrence maps for hydrogen and helium Rydberg atoms (shown for $m=0$ in Fig. 1 and for $m=1$ in Fig. 2) suggests that most of the regular structure in the spacing of the Stark energy levels persists in helium. In fact, we know from experimental studies of the helium Stark photoabsorption spectrum that the main difference is that the hydrogenic level crossings are transformed into avoided crossings for helium. Can the simple inclusion of level repulsion at these crossings account for the main differences between the hydrogen and helium recurrence maps? In particular, will this provide a mechanism that enhances the recurrence lines between the third and fourth diagonal bands of hydrogen recurrence map but has no observable effect between the first and second primary bands?

Level repulsion will mix some of the ''blue'' and ''red'' levels. The strongly repelling levels are no longer associated with the ''red'' or ''blue'' familes of substates preserved by the distant levels. In addition, the maximally repelling levels will maintain a new spacing that is one half the average of the ''red'' and ''blue'' spacings alone. Therefore, maximal repulsion will lead to new families of (''purple'') substates with mean spacings approximately equal to half the average spacing of the ''blue'' and ''red'' substates alone, $2\delta^p=\frac{1}{2}(|\delta^+|+|\delta^-|)$. In this case, the contributions from these close levels will be destructive until $k2\delta^p/\Delta_{\pm}$ is close to an integer. Therefore, we expect to get a new band of constructive interference due to the level repulsion that lies between the third and fourth hydrogenic bands centered at a scaled action of

$$s^p=1/2\delta^p=2/(|\delta^+|+|\delta^-|), \tag{25}$$

while the surrounding hydrogenic bands are diminshed in amplitude. The results of this simple estimate of the effects of avoided crossings on the helium Stark recurrence map are shown in Fig. 6(c), which agrees very well with the measured results for both the singlet and triplet states of $m=0$ helium shown in Figs. 1(b) and 1(c).

A careful examination of our helium photoabsorption spectrum supports this simple picture for the origin of the

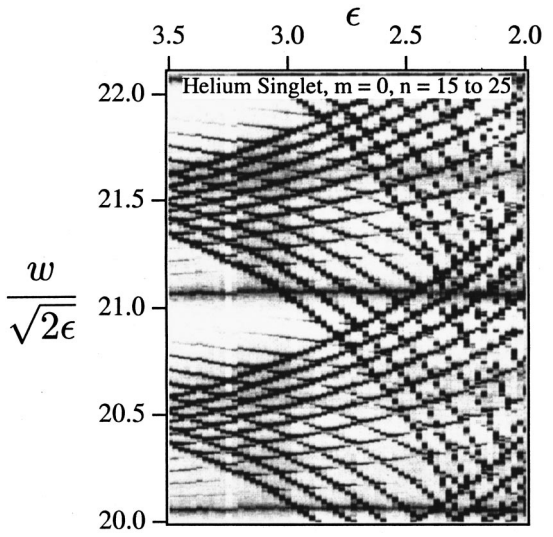

FIG. 10. The measured scaled Stark photoabsorption spectrum for $m=0$ states of helium with $n=20$–22 and ϵ ranging from 3.5 to 2 showing many avoided crossings.

new band of enhanced lines in the $m=0$ recurrence spectrum. Consider, for example, the case of $\epsilon=3.5$ where the new helium bands in the recurrence spectrum in Figs. 1(b) and 1(c) are most pronounced near the scaled action of 12 which is the value of s^p predicted by Eq. (25). The corresponding scaled photoabsorption spectrum for helium, singlet $n=20$–22 is shown in Fig. 10. This complex spectrum arises from the overlap of the near extremal ''red'' and ''blue'' levels from adjacent Stark manifolds. In hydrogen, these overlapping levels would simply cross without distortion and the corresponding spacings in the ''red'' and ''blue'' states would be separately preserved. However, in helium the nearby levels repel while the distant levels are largely undisturbed from their hydrogenic spacings.

To further test our simple picture for the origin of the helium band, we divided the scaled photoabsorption spectrum into two segments corresponding to low $n=15$–20 and high $n=20$–25. For the low $n=15$–20, the Stark manifolds have barely begun to overlap for $\epsilon=3.5$ and so most of the ''red'' and ''blue'' substates will maintain their hydrogenic spacing. In contrast, the Stark manifolds for high $n=20$–25 are strongly overlapping and the strong level repulsion shown in Fig. 10 should lead to many level spacings that are approximately one half the ''red'' or ''blue'' spacings. The corresponding recurrence spectra generated by Fourier transforming these two segments of the photoabsorption spectrum are shown in Fig. 11. These results confirm that for low $n=15$–20 the recurrence spectrum is largely hydrogenic. There are two bands of enhanced peaks near the predicted scaled actions $s_0^-=5$ and $s_0^+=7$ for the hydrogenic substate periodicities, Eq. (24), and near the first harmonics at $2s_0^-=10$ and $2s_0^+=14$. Only a small peak appears between the two hydrogenic bands at $s^p(3.5)=12$. In contrast the recurrence spectrum for high $n=20$–25 shows a broad band centered at $s^p(3.5)=12$ with a commensurate decrease in the hydrogenic bands on either side. (Note that there is no preceding band at $s=6$, so this new high frequency band

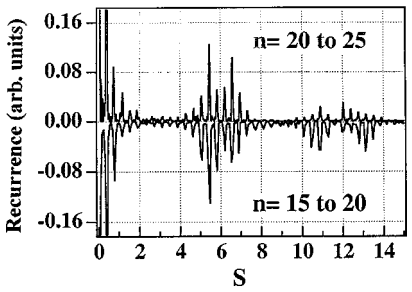

FIG. 11. The recurrence spectrum for helium $n=20$–25 (top) is compared with the more hydrogenic recurrence spectrum for helium $n=15$–20 (bottom) for $\epsilon=3.5$.

corresponds to a new periodicity in the helium photoabsorption spectrum.)

V. SUMMARY

We have studied the problem of a Rydberg atom in a uniform electric field. Using an analysis based on the quantum regularities in the scaled Stark photoabsorption spectrum, we can account for much of the fine-scale and large-scale structure of the measured scaled Stark recurrence spectrum for both hydrogen and helium Rydberg atoms. This analysis provides a simplifying description for both the $m=0$ recurrence maps, which have been previously treated using the semiclassical closed orbit theory and the $m=1$ recurrence maps for which the semiclassical closed-orbit theory breaks down.

This paper shows how the structures in the recurrence spectrum arise from the collective interference properties of the level periodicities in the quantum photoabsorption spectrum and points out that the key differences between hydrogen and helium are a direct result of the avoided level crossings in the $m=0$ helium Stark spectrum. In particular, the new band of recurrence peaks in the helium recurrence spectrum that have been previously interpreted as due to contributions of classical orbits that scatter off of the nonhydrogenic core, are here shown to arise from a new periodicity in the Stark spectrum due to large avoided crossings. This re-

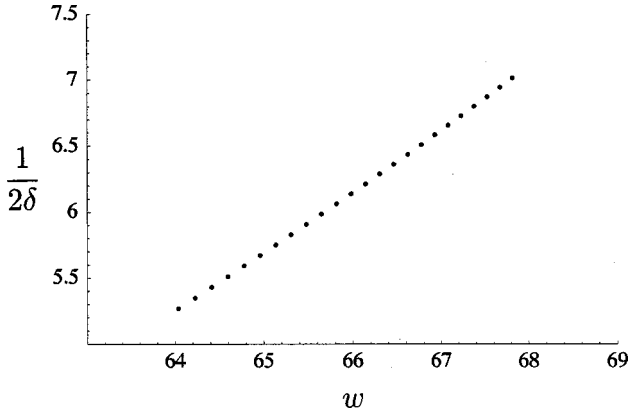

FIG. 12. The scaled Stark substate spacing frequency, $1/2\delta$, as a function of w for the $n=25$ manifold increases gradually from $s_0^-=1/2|\delta_0^-|\approx 5$ to $s_0^+=1/2|\delta_0^+|\approx 7$ for $\epsilon=3.5$.

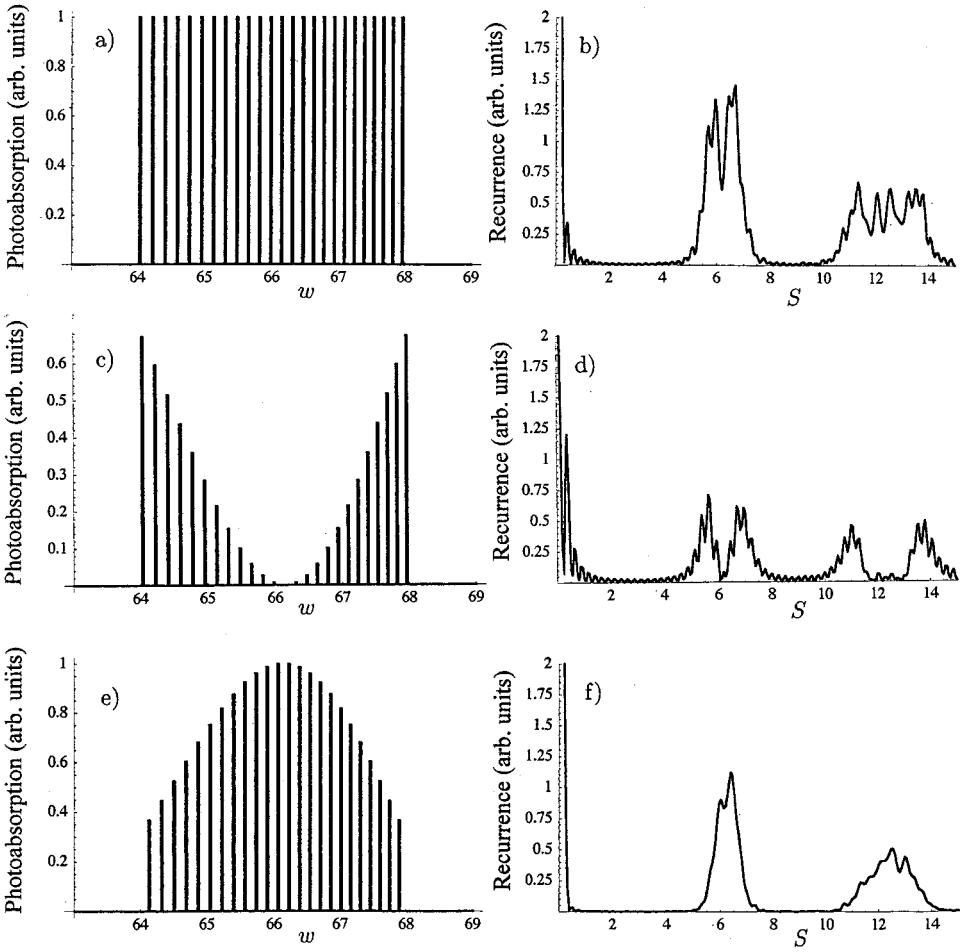

FIG. 13. (a) The $n=25$, $m=0$, scaled hydrogen Stark manifold with $\epsilon=3.5$ is displayed as a stick photoabsorption spectrum with uniform oscillator strengths. (b) The direct Fourier transform of the uniform strength spectrum in (a) shows single broad bands between the minimum and maximum substate spacing frequencies, $s_0^- = 5$ to $s_0^+ = 7$, shown in Fig. 12 and between their harmonics, 10 and 14. (c) The $n=25$, $m=0$, scaled hydrogen Stark manifold is displayed with $m=0$ oscillator strengths. (d) The direct Fourier transform of the $m=0$ photoabsorption spectrum in (c) shows the characteristic double band recurrence structure. (e) The $n=25$, $m=1$ hydrogen Stark manifold is displayed with $m=1$ oscillator strenths. (f) The direct Fourier transform of the $m=1$ photoabsorption spectrum in (e) shows the characteristic single band recurrence structure.

sult points to an interesting correspondence between classical core scattering and quantum avoided crossings that is deserving of further study.

In the $m=1$ case the classical-quantum correspondence is more subtle since real classical closed orbits that start and end at the nucleus are excluded by the angular momentum barrier at the nucleus. Our analysis of the quantum periodicities in the scaled photo-absorption spectrum for $m=1$ still provides an excellent description of the recurrence maps for both hydrogen and helium. However, the semiclassical theory requires modification. Several different semiclassical approaches to this problem are currently being pursued. First, Robicheaux and Shaw [20] have found the heuristic use of $m=0$ closed orbits to calculate the $m=1$ recurrence spectrum to be surprisingly successful, which suggests that straightforward modification of the closed-orbit theory may be in order. Second, Main [21] has shown that the extension of the classical dynamics to include ''ghost orbits'' [22] can successfully account for features in the recurrence spectrum for which there are no real classical orbits. Ultimately, both of these semiclassical approaches must be reconciled with the results of our simple analysis of the periodicities of the quantum photoabsorption spectrum that underly the structures in the recurrence spectrum.

Finally, a further test of both the quantum and semiclassical analyses will be a simple description of the regular modulations of the second, third, and fourth bands in the experimental $m=1$ helium triplet recurrence spectra shown in Fig. 2(c) that were first observed by Keeler and Morgan [13]. (These regular modulations have also been seen in recent measurements and quantum calculations of the sodium recurrence maps by Jones *et al.* [23].) We already have strong indications that these modulations can also be traced to the avoided crossings in the helium Stark spectrum. For $m=1$, the size of the avoided crossing remains small; however, there are dramatic changes in the oscillator strengths of the two avoiding levels that appear to have a significant effect on the structure of the helium recurrence spectrum [24]. Is there also a correspondence between these features of the quantum avoided crossings and core-scattered classical orbits in a semiclassical treatment of the $m=1$ case? These are future challenges that must be met by the quantum and semiclassical theories as the experiments progress to more complicated recurrence spectra of complex atoms and even to molecules in strong static fields.

ACKNOWLEDGMENTS

This work was supported by the National Science Foundation through Grant Nos. PHYS-9732458 and PHYS-9900746.

APPENDIX: DIFFRACTION FUNCTIONS FOR GRATINGS WITH NONUNIFORM SLIT SPACINGS

The origin of the double bands of constructive interference for $m=0$ and the single bands for $m=1$ can be easily understood by examining the diffraction function for a diffraction grating with graduated slit spacings. In a single n manifold, the spacings of the substates in the scaled Stark spectrum are largest near the bottom (red) end of the manifold and decrease gradually to the top (blue) end leading to the increasing substate frequencies shown in Fig. 12.

If we Fourier transform the scaled spectrum for a single $n=25$ manifold with uniform oscillator strength shown in Fig. 13(a), this variation in the spacings leads to a diffraction function with a continuous band of frequencies between the inverse of the largest spacing to the inverse of the smallest with an additional band at the second harmonics shown in Fig. 13(b). This graduated diffraction grating therefore provides a sharp bandpass filter rather than the conventional single-frequency filter provided by equally spaced slits.

Now if we weight the spectrum with the oscillator strengths for the $m=0$ and $m=1$ photoabsorption shown in Fig. 4 (top and bottom, respectively), then the Fourier transform of the $m=0$ stick photoabsorption spectrum shown in Fig. 13(c) breaks the diffraction band in Fig. 13(d) into two bands and the Fourier transform of the $m=1$ stick photoabsorption spectrum in Fig. 13(e) contracts the diffraction band in Fig. 13(f) to a single narrow band. In both cases, the shape of the envelopes for the recurrence spectrum are a direct reflection of the shape of the photoabsorption oscillator strengths. These weighted diffraction functions for graduated diffraction gratings provide a more precise definition of the envelope for the constructive and destructive interference in the $m=0$ and $m=1$ Stark recurrence spectra that are in excellent agreement with the band locations and widths in Figs. 1 and 2.

It is interesting to note that this analysis of the diffraction functions for graduated diffraction gratings, that was originally motivated by the need for a simple description of the large-scale structure for the experimentally measured Stark recurrence spectra, suggests a novel design for an optical diffraction grating that preferentially scatters or transmits a specified band of frequencies—just gradually vary the slit spacings across the grating to span the desired frequencies.

[1] E. Heller and S. Tomsavic, Phys. Today **46(7)**, 38 (1993).

[2] M. C. Gutzwiller, *Chaos in Classical and Quantum Mechanics* (Springer, New York, 1991); M.C. Gutzwiller, J. Math. Phys. **12**, 343 (1971).

[3] M.V. Berry and M. Tabor, Proc. R. Soc. London, Ser. A **249**, 101 (1976).

[4] J. Gao and J.B. Delos, Phys. Rev. A **49**, 869 (1994).

[5] M.L. Du and J.B. Delos, Phys. Rev. A **38**, 1896 (1988).

[6] E.J. Heller, Phys. Rev. Lett. **53**, 1515 (1984).

[7] J. Main, G. Wienbush, A. Holle, and K.H. Welge, Phys. Rev. Lett. **57**, 2789 (1986).

[8] J. Main, G. Wiebusch, K. Welge, J. Shaw, and J.B. Delos, Phys. Rev. A **49**, 847 (1994).

[9] G.R. Welch, M.M. Kash, C. Iu, L. Hsu, and D. Kleppner, Phys. Rev. Lett. **62**, 1975 (1989).

[10] M. Courtney, H. Jiao, N. Spellmeyer, and D. Kleppner, Phys. Rev. A **51**, 3604 (1995).

[11] A. Kips, W. Vassen, and W. Hogervorst, Phys. Rev. A **59**, 2948 (1999).

[12] A. Kips, W. Vassen, W. Hogervorst, and P.A. Dando, Phys. Rev. A **58**, 3043 (1998).

[13] M.L. Keeler and T.J. Morgan, Phys. Rev. Lett. **80**, 5726 (1998).

[14] M.L. Keeler and T.J. Morgan, Phys. Rev. A **59**, 4559 (1999).

[15] M. L. Keeler, Ph.D. Dissertation, Wesleyan University, 1998.

[16] V. Kondratovich and J.B. Delos, Phys. Rev. A **57**, 4654 (1998).

[17] V. Kondratovich and J.B. Delos, Phys. Rev. A **57**, 4604 (1998).

[18] Yet another approach to understanding the recurrence spectrum is provided by the work of Wals and van den Heuvell [J. Wals and H.B. van Linden van den Heuvell, J. Phys. B **30**, 941 (1997)] who argue that the enhanced recurrence peaks for $m=0$ can be understood in the time domain as a quantum resonance between the periods of the angular librational motion of the electron wavepackets, $\tau_{ang}^{bl,rd}$, and the periods of radial oscillations of the electron wavepackets, $\tau_{rad}^{bl,rd}$, that track the classical uphill (blue) and downhill (red) orbits in the static electric field. Since the classical bifurcations are expected to occur when the radial and angular periods are commensurate, the classical and quantum correspondence between the bifurcation points and the enhanced recurrence strengths is clear. Then the resonance condition $k\tau_{rad}^{bl,rd}=m\tau_{ang}^{bl,rd}$ predicts enhanced recurrence peaks for scaled actions and scaled energies, $\epsilon^{bl,rd}=(\sqrt{3}/2)[|(k\mp 2m)|/\sqrt{m(k\mp m)}]$, that are identical to those given by Eq. (18), where $k\equiv s_0^{\pm}/S_0^{\pm}$ for the blue $(+)$ and red $(-)$ states, respectively, and $m=1$ for the first pair of red and blue bands in Fig. 1, $m=2$ for the second pair of bands, and so on. Unfortunately, the results of Wals and van den Heuvell's analysis are incorrectly plotted in their Fig. 4 due to an erroneous association of the k and m indices with the u and v periods that label the closed orbits. In Fig. 4 of Wals and van den Heuvell the upper solid curve is correct but the lower curve should not pass through the exact 1/2 classical bifurcation point at $\epsilon=2$ and should lie above all of the classical bifurcation points.

[19] J.A. Shaw and F. Robicheaux, Phys. Rev. A **58**, 1910 (1998).

[20] F. Robicheaux and J. Shaw, Phys. Rev. A **58**, 1043 (1998).

[21] J. Main, Phys. Rev. A **60**, 1726 (1999).

[22] T. Bartsch, J. Main, and G. Wunner, J. Phys. A **32**, 3013 (1999).

[23] S.N. Pisharody, J.G. Zeibel, and R.R. Jones, Phys. Rev. A **61**, 063405 (2000).

[24] H. Flores, D. Wright, R. V. Jensen, and T. Morgan (unpublished).